Non-Linear Primary Control Mapping for Droop-Like Behavior of Microgrid Systems

Martin Legry, Jean-Yves Dieulot, Frederic Colas, Christophe Saudemont, Olivier Ducarme

Non-Linear Primary Control Mapping for Droop-Like Behavior of Microgrid Systems

Martin Legry, *Member, IEEE*, Jean-Yves Dieulot, Frédéric Colas, *Member, IEEE*, Christophe Saudemont, and Olivier Ducarme

***Abstract*—Interconnecting microgrids in LV power system presents appealing features such as self-healing or power quality. When networked microgrids are not connected to a strong utility grid, their Point of Common Coupling (PCC) voltage and their power reserves vary with the operating point. An external droop control architecture is proposed that allows active and reactive power sharing among the different microgrids, thereby stabilizing the system frequency and PCC voltage, and the maximum achievable droop gains are supplied. Next, the design of appropriate primary controllers for the Distributed Energy Resources inside each microgrid allows to achieve a specified aggregated external droop controller at the connection point with little communication requirements. This methodology is applied to a modified CIGRE benchmark and shows good results while keeping a standard decentralized control architecture.**

***Index Terms*—Networked microgrids, DER primary control, nonlinear primary control, PCC doop control.**

NOMENCLATURE

$\mathcal{R}$	Set of grid nodes
$\mathcal{R}_d$	Set of inverter-controlled nodes
ω	System frequency
ω^n	Nominal system frequency
V_i	Voltage magnitude of node i
V_i^n	Nominal voltage magnitude of node i
θ_i	Phase angle of node i
P_i Q_i	Active and reactive power at node i
P_i^0 Q_i^0	Initial active and reactive power at node i
$(\cdot)_i^g$	Variable $(\cdot)$ related to the generation at node i
$(\cdot)_i^l$	Variable $(\cdot)$ related to the load at node i
P_i^{ref} Q_i^{ref}	Active and reactive power references at node i
k_{pcc}^p	Active power droop coefficient at PCC
k_{pcc}^q	Reactive power droop coefficient at PCC
G_{ij} B_{ij}	Real and imaginary part of the bus admittance matrix of the line ij
S_{base}	Apparent base power
$\Delta P_i \Delta Q_i$	Modulated active and reactive power at node i
$\overline{(\cdot)}$	Maximum allowed of variable
$\underline{(\cdot)}$	Minimum allowed of variable
$\hat{(\cdot)}$	Expected value of variable $(\cdot)$.
λ_p λ_q	Weighting factors.

I. INTRODUCTION

MICROGRIDS are considered as a way to increase the penetration of renewable Distributed Energy Resources (DER) [1]. They are able to work in islanded mode or supporting a distribution grid. The traditional hierarchy of controllers in a standard microgrid has three layers [2]. The primary control, generally droop-based, is designed to stabilize the grid frequency and voltage by using only local measurements and local DER controllers. The secondary control of the microgrid is an Energy Management System which yields the references of the primary control and is commonly achieved by optimization-based algorithms. The purpose of tertiary control is to manage the power flow between the microgrid and the utility grid and coordinate, whenever appropriate, the operation of grid-connected microgrids. The interconnection of several microgrids to form a networked microgrid system presents appealing features such as self-healing capabilities, load control or power quality to the distribution grids [3]. However, the interactions and cooperation between microgrids or more generally clusters with DER and local intelligence in such a system make think microgrid control anew [4]. Cooperation and tertiary control may enable market bidding and energy-based transactions. It has been largely covered by the literature as a reformulation of the classical unit commitment (UC) or economic dispatch (ED) optimization problem, see for example [5], [6], [7] and the references therein. Unlike the case of the connection to a strong grid which is well-covered in the literature, the problem is to find how power can be shared among networked weak microgrids. Primary control and automatic control of the power flow through tie lines are of major concerns. This task can be completed by back-to-back converters [8] or smart transformers [9], [10], [11] at the expense of microgrids cost and converters losses. However, for networked microgrids, one can use static switches and synchronization routines at the price of weak flexibility to manage the interface which is the alternative this paper focuses on.

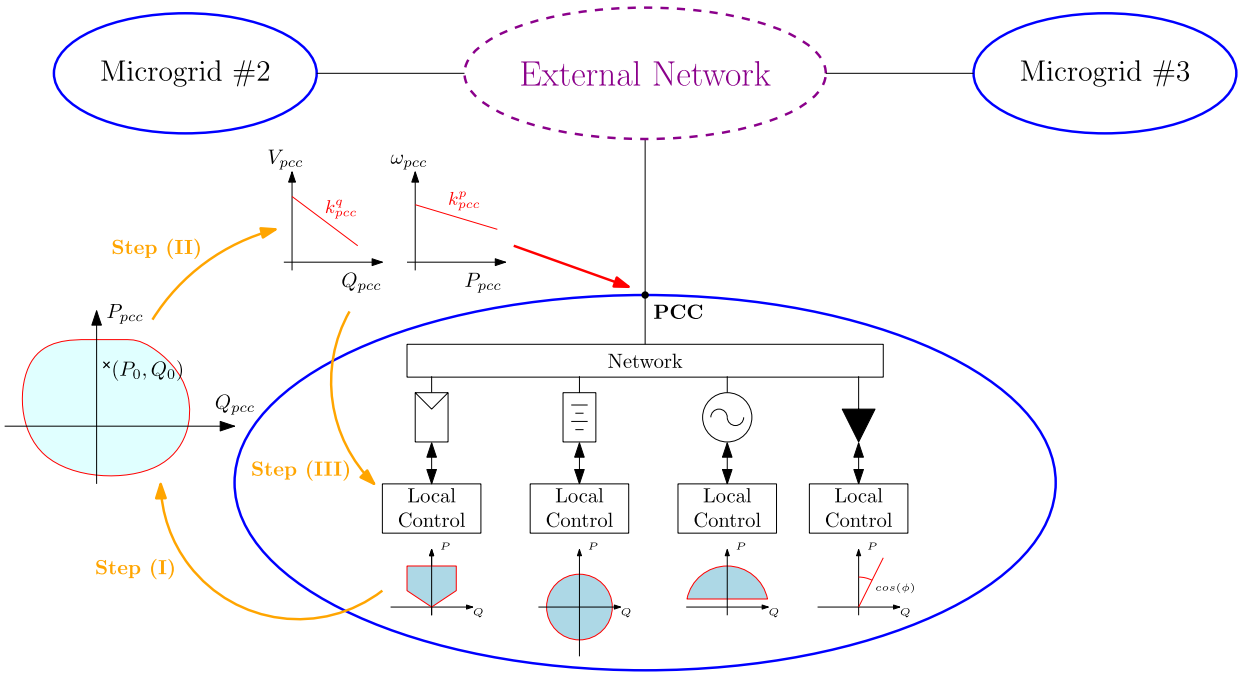

Fig. 1. General synoptic of droop-like behaviour of the PCC by optimally tuning local non linear primary controllers — (1) flexibility aggregation, (2) virtual PCC droop gains, (3) local control laws synthesis.

Nonetheless, creating a networked microgrid system may lead to changes in power flows and increase losses and the cost of energy. References [12] and [13] proposed a routine to adapt the power sharing among supporting microgrids. The algorithm computes new droop coefficients, according to the mismatch between the total and desired flows of the tie-line, while ensuring the stability and the consistency of the decentralized local droops. Reference [14] introduced an adaptive modified droop for controlling frequency, when connected through a tie-line converter or for networked microgrids. Still, no specific attention was given to the PCC behavior. Reference [15] proposed a Model Predictive hierarchical controller which embeds a Virtual Power Plant (VPP) into the frequency control scheme. The primary control allocates the power demand between the different levers using an optimization routine, but the internal power system is neglected in the model. Reference [16] designed a joint economic dispatch and power flow optimization which minimizes a reference tracking cost and providing a synthesis of the local control laws for each DER. However, the algorithm requires to receive an external signal from an independent operator and no implicit behavior is enforced at the PCC. Reference [17] introduced the Technical VPP (TVPP) as an extension of the VPP concept that aggregates and models the characteristics of a system with DERs. Still, to the best of the authors' knowledge, no further publications deal with an automatic control of the primary control for TVPP. In the literature, nothing is proposed to enforce any specific power sharing policy at the microgrid PCC. One of the most promising methods aims to define local controls of Heating, Ventilation and Air-Conditioning (HVAC) units [18]. The objective is to determine the ON/OFF triggers of HVAC according to frequency references. Under comfort and over actuation constraints, the algorithm results into a virtual P-f droop curve of HVAC aggregation. As for every direct load control modulation of active power, it is based on ON/OFF triggers that do not consider DER control. In order to obtain a specific behavior at the PCC and to ensure a power sharing policy, a first solution would be to consider a centralized supervision strategy based on an external signal. Instead, this paper proposes a hierarchical framework using load and generation flexibilities to optimally tune non linear local controllers in order to provide an automatic primary response at the PCC. The general principle is depicted in Fig. 1. The general capability of the microgrid is estimated (I), and based on global coordination and capabilities, the maximum achievable droop gains at the PCC are obtained (II). Finally, the primary control laws are determined to enforce the specific droop-like behavior at the PCC (III).

The resulting control structure exhibits the following advantages and novelties:

- No external signal is required at the PCC to enforce a microgrid primary controller;
- The primary response at the PCC is optimally distributed among the flexibilities (DERs) considering their heterogeneities, constraints and limitations. The nonlinear primary control of the DERs requires only the PCC voltage and frequency signals, and is quite different from the conventional local droop architecture;
- The external operator (DSO or coordinator) only requires to know the capabilities and the behavior enforced at the PCC, preserving data and operating privacy.

The remainder of this paper is organized as follows. First, based on an extension of the literature on the flexibility aggregation, a routine to determine the global flexibility for different voltage is proposed in Section II which yields the microgrid capabilities and droop gains. Section III addresses

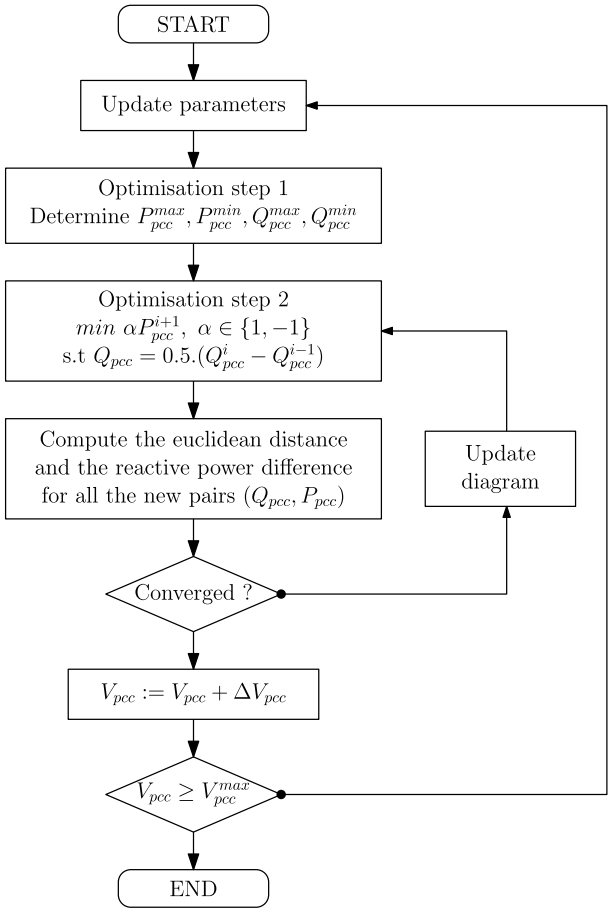

Fig. 2. Flexibility aggregation routine for variable PCC voltage.

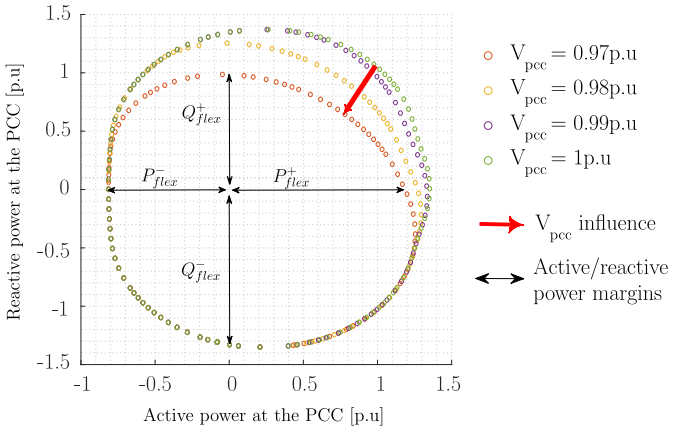

Fig. 3. Capability diagram of a 2-flexibility microgrid.

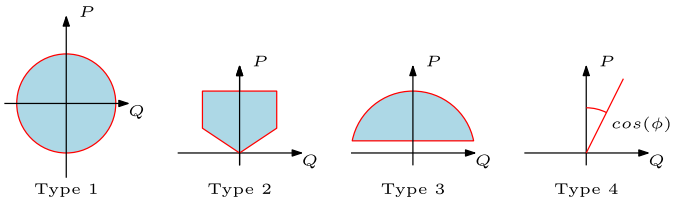

Fig. 4. Unitary flexibility diagrams.

the synthesis of the nonlinear mapping of the active and reactive power of each DER as an optimal problem. Finally, the proposed framework is validated by simulation in Section IV on a modified European LV distribution benchmark network.

The proposed methodology aims to support active and reactive powers at the PCC within the framework of primary control mechanism. Usually, this action takes place within few seconds, for at least few minutes. A recent update of the German grid codes requires a change in the reactive power set point to be reached in 6 to 60 seconds [19]. The following developments consider a three-phase balanced network and assume the voltage to be a true sine wave, and therefore, the PCC distortions and power electronics non-linearities are not considered.

II. PCC Behavior of Networked Microgrids

A. Flexibility Aggregation and Equivalent PQ Diagram

Microgrid operators must be able to quantify the reserves of the system in a similar manner that for a single inverter through a capability diagram. Therefore, based on the unitary capability diagrams, the routine presented in Fig. 2 aims to determine the aggregated capability at the PCC for each microgrid. Fortunately, a number of recent papers have addressed this point when a sub-part of a grid is connected to a distribution grid with a nonlinear formulation of the power flow problem [20] or based on a linearization of the Optimal Power Flow (OPF) equations [21]. However, in Low Voltage and weak power systems, PCC voltages are highly fluctuating, and, in turn, any change in the power injections from the microgrid to the external network will induce in a change in the PCC voltage, due to the power sharing between the networked microgrids. This behavior is highlighted in Fig. 3 which presents a diagram for a simple 2-flexibility microgrid. Therefore, in networked microgrid systems, the aggregation of flexibilities should consider a wide range of PCC voltages and should be estimated in real time. Hence, the aggregation routines proposed in the aforementioned papers has been updated to the case where the PCC voltage varies. Specifically, the method proposed in [20] can be easily extended. First, an OPF estimates the maximum and minimum reachable active and reactive powers at the PCC. This results in four couples (P^i, Q^i) with $i \in \{1,2,3,4\}$. In a second step, an OPF minimizes

$$\alpha P_{pcc}^{i+1}, \text{ and } i \geq 4, \alpha \in \{1,-1\}.$$

The reactive power is constrained to the mean value of the reactive power between two successive points $Q_{pcc}^{i+1} = 0.5 \times (Q_{pcc}^{i} - Q_{pcc}^{i-1})$. Then, the minimum or maximum active power can be found respectively for $\alpha = 1$ and $\alpha = -1$. The algorithm iterates for each new pair of points until the distance between two successive points is less than a prescribed tolerance, and the routine is repeated for the full range of PCC voltages. The resulting figure is a diagram that maps the active and reactive power flexibilities according to the voltage at the PCC. The flexibilities are assumed to be ideal and characterized by a unitary PQ diagram (see Fig. 4) and their dynamics are discarded. These diagrams may present slight differences,

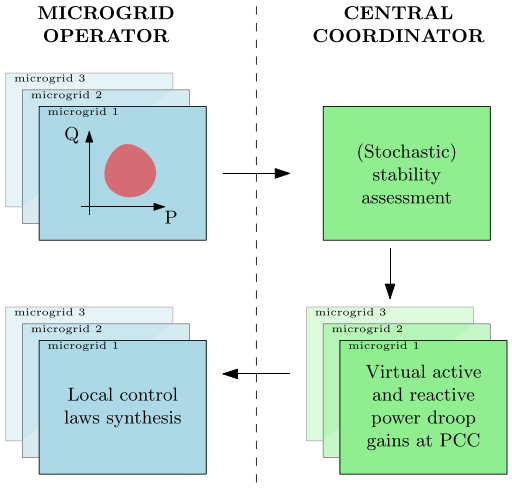

Fig. 5. Global architecture and coordination of networked microgrids.

such as for the wind turbine generators, or synchronous generators in which the excitation systems may reduce the reactive power capabilities [22]. However, the diagrams are not significantly modified, and the proposed methodology remains valid as long as the diagrams are convex, which is generally the case. Type 1 represents an ideal energy storage system (ESS), constrained by its output current, type 2 represents a renewable system, able to de-rate its output power, type 3 models a conventional generator (see [23, Figs. 1 and 2]), constrained by its output current and by a minimal output active power, and type 4 models a flexible load. Finally, the modified algorithm is depicted in Fig. 2.

B. Architecture and Coordination of Networked Microgrids System

To discuss the architecture and the coordination technique between the microgrids is beyond the scope of this paper. Still, Fig. 5 exhibits the architecture considered in the following with a coordination agent that assesses the stability of the networked microgrid system to determine the necessary behavior at the different PCCs according to classical criteria (such as the N–1 situation). These gains can also be obtained through a different architecture, such as consensus-based [24]. In both cases, the specified behavior at the PCCs is assumed to be sufficient to ensure the stability of the whole networked microgrids system. The choice between conventional or opposite droop control at the PCC indeed depends on the R_{ext} versus X_{ext} ratio of the transmission line between the microgrid PCC and the external network. Numerous low voltage cables or lines favour the use of opposite droop control that relates the active power to the voltage deviation and the reactive power to the frequency deviation. However, [25] and [26] pointed out that conventional droop relations are suitable for low voltage network due to the indirect coupling between the active power and the frequency and between the reactive power and the voltage magnitude. Finally, it is important to remark that the choice of the droop relations we want to enforce at the PCC only changes the relations and the virtual droop coefficients in the objective function. In the remainder it is assumed that the stability is ensured with a conventional droop law at the PCCs:

$$\begin{aligned} P_{pcc} - P_{pcc}^{ref} &= -k_{pcc}^{p}.\left(\omega - \omega^{n}\right), \\ Q_{pcc} - Q_{pcc}^{ref} &= -k_{pcc}^{q}.\left(V_{pcc} - V_{pcc}^{n}\right). \end{aligned} \tag{1}$$

C. Variable PCC Droop Control for Weak Networks

In this section a method to determine the maximum achievable droop gains k_{pcc}^{p} and k_{pcc}^{q} is proposed. These gains can be found by considering the active and reactive power margins at the PCC and the frequency and the voltage deviations. Voltage and frequency deviations must remain within a tolerance band of five percent (see [27] type B). To support the droop gains computation, the following values are defined:

$$\begin{aligned} P_{flex}^{+} &= \max\left(P_{pcc}|Q_{pcc} = Q_{pcc}^{0}\right) - P_{pcc}^{0}, \\ P_{flex}^{-} &= \min\left(P_{pcc}|Q_{pcc} = Q_{pcc}^{0}\right) - P_{pcc}^{0}, \\ Q_{flex}^{+} &= \max\left(Q_{pcc}|P_{pcc} = P_{pcc}^{0}\right) - Q_{pcc}^{0}, \\ Q_{flex}^{-} &= \min\left(Q_{pcc}|P_{pcc} = P_{pcc}^{0}\right) - Q_{pcc}^{0}, \end{aligned} \tag{2}$$

where P_{flex}^{+} and P_{flex}^{-} are the maximum active power that the microgrid is able to modulate, and $(P_{pcc}|Q_{pcc} = Q_{pcc}^{0})$ denotes the active power P_{pcc} when the reactive power at the PCC is equal to its initial value Q_{pcc}^{0}. The same holds for the reactive power. The arrows on Fig. 3 exhibit the power margins from an initial situation without any power exchange between the microgrid and the external network.

Therefore, the droop gains at the PCC are as follows:

$$\begin{aligned} k_{pcc}^{p+} &= \frac{P_{flex}^{+}}{\underline{\omega} - \omega^{n}}, \\ k_{pcc}^{p-} &= \frac{P_{flex}^{-}}{\omega^{n} - \overline{\omega}}. \end{aligned} \tag{3}$$

In the remainder, without loss of generality, the droop is assumed to be symmetric, that is to say $k_{pcc}^{p} = \min(k_{pcc}^{p^+}, k_{pcc}^{p^-})$, and $k_{pcc}^{q} = \min(k_{pcc}^{q^+}, k_{pcc}^{q^-})$. In addition, conventional conditions for stability hold. The power sharing strategy that generates the networked microgrids droop gains is out of the scope of this paper; our method aims to calculate the maximum droop gain that can be actually achieved for a microgrid. We refer the interested readers to [28] and [29] and the references therein for more in-depth details on droop stability.

Finally, the operating area defined by the droop control (1) is a rectangle as can be seen in Fig. 6. However, some small regions of the rectangle are outside of the capability diagram (hatched areas in Fig. 6) which means that the corresponding operating point cannot be reached. A solution would have been to reduce drastically the active and reactive power margins. This would generate a smaller rectangle that would fit into the capability diagram, thereby yielding lower maximum achievable droop coefficients. However, the methodology detailed in the next section proposes to handle this situation through the formulation of an objective function.

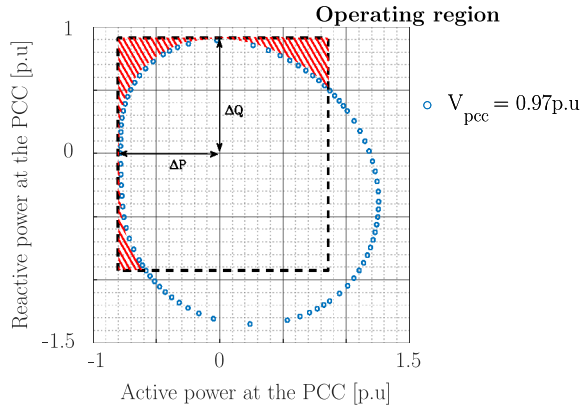

Fig. 6. Resulting operating region of a 2-flexibility microgrid with $V_{pcc} = 0.97$ pu.

III. External Droop Control Achievement via DER Local Controller Synthesis

A. Structure of Local Control Laws

The local controllers of the flexibilities of a microgrid are the only degrees of freedom which enable to enforce a droop-like behavior at the PCC (3), which considers only the frequency and PCC voltage. Hence, a new methodology is required to determine the primary control laws of the DERs f_i and g_i, that will be based on these two variables, contrary to the traditional local droop controllers that use the local node voltages. The resulting mapping will be nonlinear because of the power flow equations:

$$\begin{aligned} P_i^g &= P_i^{ref} + f_i(\omega, V_{pcc}), \\ Q_i^g &= Q_i^{ref} + g_i(\omega, V_{pcc}). \end{aligned} \tag{7}$$

By combining the conventional power flow equations to the desired behavior at the PCC (4) and the control laws at the inverter nodes, the microgrid system can be represented by (4)-(6), as shown at the bottom of the page.

B. Optimal Tuning of DER Non-Linear Primary Control

The microgrid system presents numerous degrees of freedom thus, in order to determine suitable DER control laws, the system of (4)-(6) is solved using Non Linear Programming (NLP) methods. We recall that the DERs nonlinear primary controllers should consider the frequency and the PCC voltage to enforce a droop-like controller at the PCC. As the frequency ω is a global variable shared by all nodes, the only variable that needs to be communicated to the controllers is the PCC voltage.

The following section presents the objective function and constraints of the NLP.

Objective function: The function to be minimized should consider two main objectives. The first one consists to supply the expected active and reactive power injections at the PCC according to (1). It is important to note that the method proposed to define the droop coefficient may lead to unreachable states as previously detailed. Thus, the objective function embeds a least square problem with different weighting factors λ_p and λ_q for the active and reactive power deviation respectively, which also help to prioritize the provision of voltage or frequency support. The second objective aims to share the effort proportionally among the levers. This strategy avoids to request power only from the levers which exhibit a strong coupling with the PCC. Moreover, the EMS yields an economic optimum for the steady state, for which the criterion embeds a weighted sum of the powers quadratic deviations. Hence, in general, proportional power sharing avoids large deviations from a single lever and keeps the operating point close to the economic optimum.

This results in the following objective function

$$\begin{aligned} \mathcal{J}(\Delta\omega, \Delta V_{pcc}) = {} & \lambda_p \left\| P_{pcc}^0 - k_{pcc}^p \Delta\omega \right\|^2 \\ & + \lambda_q \left\| Q_{pcc}^0 - k_{pcc}^q \Delta V_{pcc} \right\|^2 \\ & + \sum_{i \in \mathcal{R}_d} \left(\frac{\Delta P_i}{P_i^n} S_{base} - \Delta P_{pcc} \right)^2 \\ & + \sum_{i \in \mathcal{R}_d} \left(\frac{\Delta Q_i}{Q_i^n} S_{base} - \Delta Q_{pcc} \right)^2, \end{aligned} \tag{8}$$

with ΔP_i and ΔQ_i the active and reactive power changes of the piloted node $i \in \mathcal{R}_d$.

Constraints: The constraints of the NLP are the conventional constraints of OPF, plus the flexibility diagrams as detailed in the remainder of this section.

$$P_{pcc}^{ref} - k_{pcc}^p \cdot (\omega - \omega^n) = V_{pcc} \sum_{j \in N} V_j \left(G_{pccj} \cos(\theta_{pcc} - \theta_j) + B_{pccj} \sin(\theta_{pcc} - \theta_j) \right)$$

$$Q_{pcc}^{ref} - k_{pcc}^q \cdot \left(V_{pcc} - V_{pcc}^n \right) = V_{pcc} \sum_{j \in N} V_j \left(G_{pccj} \sin(\theta_{pcc} - \theta_j) - B_{pccj} \cos(\theta_{pcc} - \theta_j) \right) \tag{4}$$

$$\forall i \in \mathcal{R}_d \begin{cases} P_i^{ref} + f_i(\omega, V_{pcc}) = V_i \sum_{j \in N} V_j \left(G_{ij} \cos(\theta_i - \theta_j) + B_{ij} \sin(\theta_i - \theta_j) \right) \\ Q_i^{ref} + g_i(\omega, V_{pcc}) = V_i \sum_{j \in N} V_j \left(G_{ij} \sin(\theta_i - \theta_j) - B_{ij} \cos(\theta_i - \theta_j) \right) \end{cases} \tag{5}$$

$$\forall i \in \{\mathcal{R} - \mathcal{R}_d\} \begin{cases} P_k = V_k \sum_{j \in N} V_j \left(G_{kj} \cos(\theta_k - \theta_j) + B_{kj} \sin(\theta_k - \theta_j) \right) \\ Q_k = V_k \sum_{j \in N} V_j \left(G_{kj} \sin(\theta_k - \theta_j) - B_{kj} \cos(\theta_k - \theta_j) \right) \end{cases} \tag{6}$$

- Power flow model: The optimization problem considers the power flow equations (4)-(6) as a set of constraints. The precise model of the network with the admittance matrix Y considers the complex nature of the internal lines and their R versus X ratio are therefore intrinsically considered in the resulting local control laws.
- Nodal power balance:

$$\begin{aligned} \Delta P_i &= \Delta P_i^g - \Delta P_i^l, \ \forall i \in \mathcal{R}, \\ \Delta Q_i &= \Delta Q_i^g - \Delta Q_i^l, \ \forall i \in \mathcal{R}. \end{aligned} \tag{9}$$

- Voltage constraints:

$$\underline{V_i} \leq V_i \leq \overline{V_i}. \tag{10}$$

- Unitary capability constraints: Four types of flexibility diagrams are considered as shown in Fig. 3.
Type 1:

$$\begin{aligned} \underline{P_i} \leq P_i^g \leq \overline{P_i}, \\ \left(P_i^g\right)^2 + \left(Q_i^g\right)^2 \leq \overline{S_i}. \end{aligned} \tag{11}$$

Type 2:

$$\begin{aligned} 0 \leq P_i^g \leq P_i^{g0}, \\ -0.36 \leq Q_i^g \leq 0.36, \\ -0.36 \times \frac{P_i^{tr} - P_i^g}{P_i^{tr}} \leq Q_i^g \leq 0.36 \times \frac{P_i^{tr} - P_i^g}{P_i^{tr}}, \end{aligned} \tag{12}$$

with P_i^{tr}, the minimal active power to provide full reactive power support.
Type 3:

$$\begin{aligned} \delta_i \underline{P_i} \leq P_i^g \leq \delta_i \overline{P_i}, \\ \left(P_i^g\right)^2 + \left(Q_i^g\right)^2 \leq \delta_i \overline{P_i}, \end{aligned} \tag{13}$$

with $\overline{P_i}$ and $\underline{P_i}$, the maximal and minimal output active power of the generator when started, and δ_i a Boolean which states whether the diesel generator is running or not. However, the start up or shut down of a type 3 flexibility is not considered.
Type 4:

$$Q_i = P_i \cos(\phi_i). \tag{14}$$

Last, there may be generating units for which the local control laws cannot be updated such as droop-controlled inverters. For these units, an additional set of constraints accounts for their behavior, as

$$\begin{aligned} P_i &= P_i^{ref} + k_i^p \Delta\omega, \\ Q_i &= Q_i^{ref} + k_i^q \Delta V_i. \end{aligned} \tag{15}$$

Finally, the optimization problem can be summarized as:

$$\begin{aligned} \min_{\Delta\mathbf{P_i}, \Delta\mathbf{Q_i}, i \in \mathcal{R}_d} \quad & J\left(\Delta\omega, \Delta V_{pcc}\right) \\ \text{s. t.} \quad & (4) \text{ - } (15) \end{aligned} \tag{16}$$

The overall flowchart is depicted in Fig. 7.

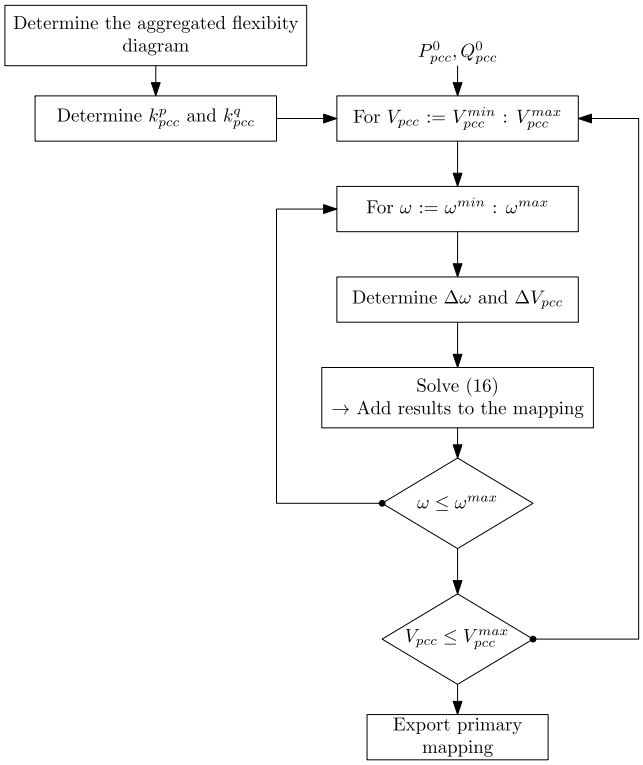

Fig. 7. DER primary control design procedure.

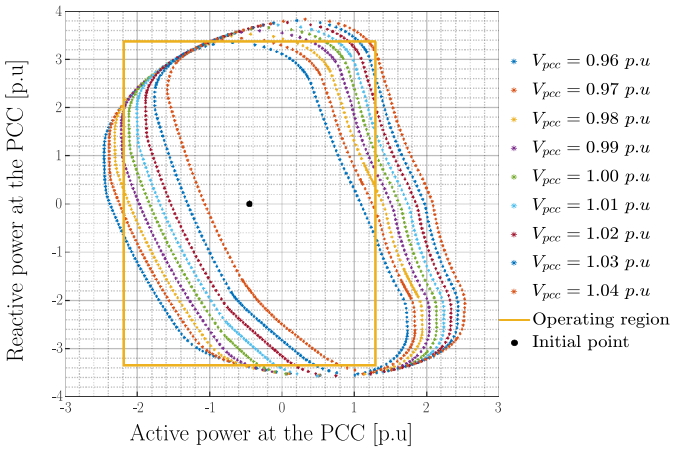

Fig. 8. Flexibility diagram of the 18-node modified European LV benchmark network.

IV. Simulation Results and Discussion

The simulations use a modified version of the CIGRE European LV residential distribution network benchmark [30], which parameters are detailed in Table II–V. The network described in Fig. 9 includes two storage systems (type 1, see Fig. 4), two photo-voltaic (PV) plants (type 2) and a conventional generator (type 3). From now on, a positive power indicates a generation, while a load is labeled as negative. The external network is considered as a load at the PCC (see Fig. 9).

The initial operating point of the microgrid is given in Table V. Following the methodology summarized in Fig. 7,

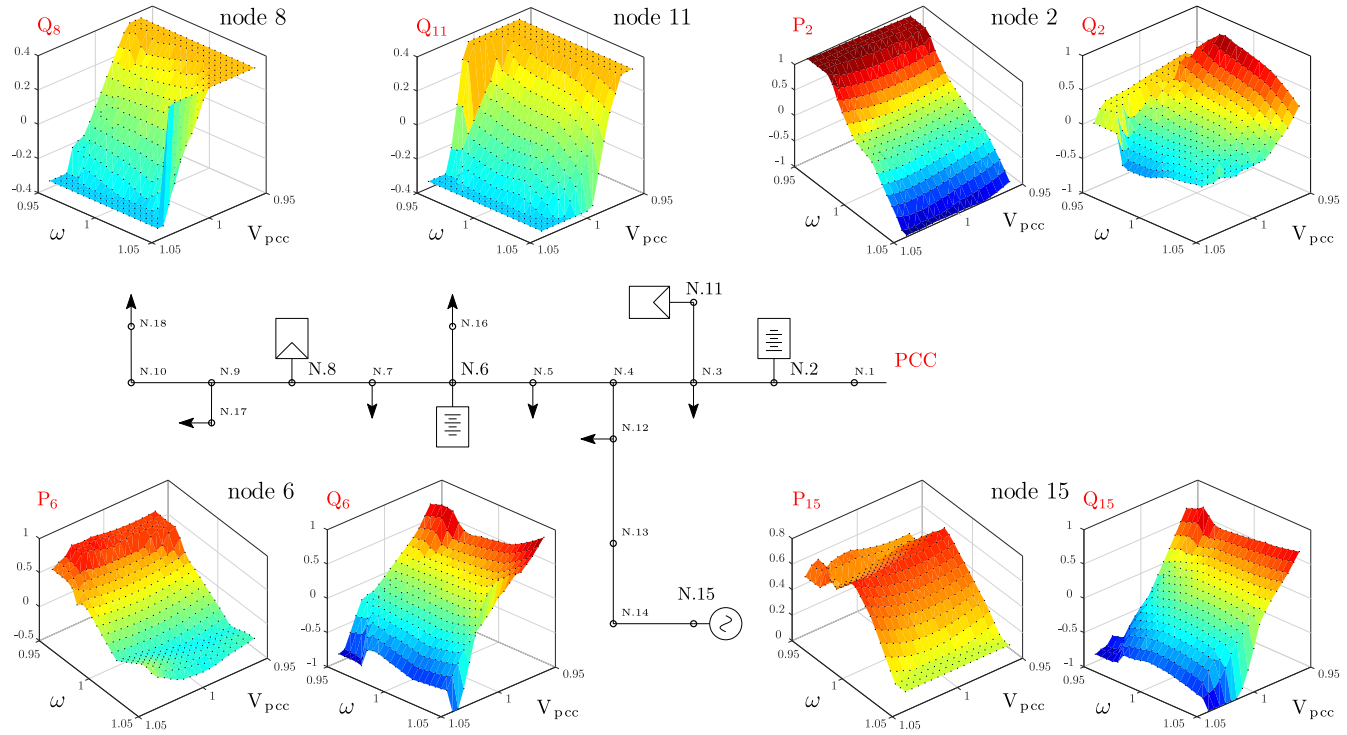

Fig. 9. Microgrid topology — Flexibilities and resulting primary mapping $P - \{\omega, V_{pcc}\}$ and $Q - \{\omega, V_{pcc}\}$.

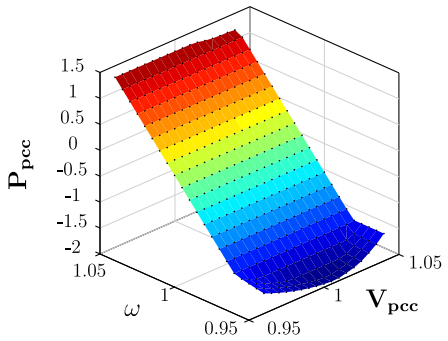

Fig. 10. Resulting active power behavior at the point of common coupling- $P_{pcc} - \{\omega, V_{pcc}\}$.

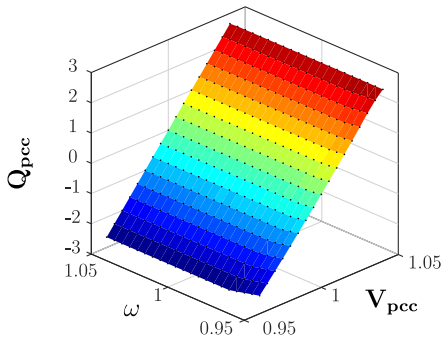

Fig. 11. Resulting reactive power behavior at the point of common coupling - $Q_{pcc} - \{\omega, V_{pcc}\}$.

the capability diagram at the PCC (Fig. 8) can be inferred from the flexibility diagrams of the DERs.

The shape of the capability diagram depends mainly on the grid topology and the DERs flexibilities, but is quite robust with respect to the initial operating point. Equation (2) gives the power margins $\Delta P = 1.75$ pu and $\Delta Q = 3.43$ pu corresponding to the rectangle centered on $P^0_{pcc} = 0.45$ pu, $Q^0_{pcc} = 0$ pu. The maximum achievable droop coefficients $k^p_{pcc} = 34.6$ and $k^q_{pcc} = 68.6$ are calculated from (3). The results presented in this section consider the maximum droop coefficients.

A. Complete Control of DERs

Fig. 10 and 11 display respectively the $P - \{\omega, V_{pcc}\}$ and $Q - \{\omega, V_{pcc}\}$ mappings obtained by the optimal tuning method of Section III-B, which are almost linear. When the operating point is outside of the PCC capability diagram, the corresponding active power injection deviates significantly from the expected linear PCC droop control law, while the reactive power injection is barely affected. This situation occurs for under frequency and extreme PCC voltages (left part of Fig. 8).

Fig. 9 also displays the nonlinear primary control mappings of the DERs, depending on V_{pcc} and ω. The diagrams display the active and reactive power injections scaled with a per unit PCC power. As a general rule, we can see that the control effort is shared proportionally among the levers. Each nonlinear control mapping can be interpreted consistently with the characteristics of the LV network and the operating constraints. A first remark is that the network is mainly resistive ($\frac{X}{R} < 1$). Hence, only a limited number of DERs exhibit a strong coupling between their active powers and the grid frequency. Specifically, an important share of the required active power at the PCC is allocated to node 2, and the corresponding diagrams are rather similar. This induces a strong constraint on

TABLE I
INFLUENCE OF λ_p AND λ_q ON THE PCC POWER INJECTIONS

λ_p	$\frac{\lambda_q}{\lambda_p}$	**Active power [pu]**	**Reactive power [pu]**	**Error on P_{pcc} [%]**	**Error on Q_{pcc} [%]**
1	1	1.612	2.406	26.35	10.2
1	2	1.558	2.526	28.82	5.66
1	100	1.489	2.675	31.95	0.13
1	0.5	1.688	2.232	22.87	16.66
1	0.01	2.142	1.059	2.16	60.46

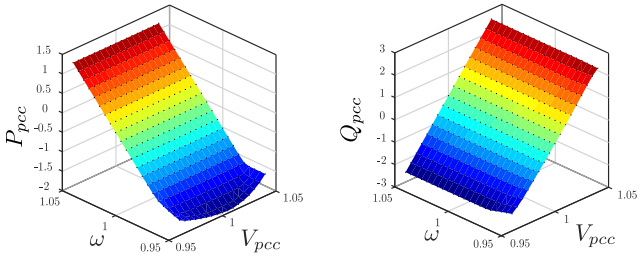

Fig. 12. Resulting active and reactive power behavior at the point of common coupling - $P_{pcc} - \{\omega, V_{pcc}\}$ and $Q_{pcc} - \{\omega, V_{pcc}\}$.

TABLE II
INITIAL OPERATING POINT

Node	**Voltage [pu]**	**Active power [pu]**	**Reactive power [pu]**
2	1.004	0.00	0.00
6	0.995	0.00	0.00
8	0.992	0.25	0.00
11	1.022	0.42	0.00
15	1.036	0.54	0.00
PCC	1.000	0.45	-0.01

TABLE III
DER PARAMETERS

Type	**Node**	**P_{nom} [kW]**	**Flexibility**
ESS	2	100	1
ESS	6	100	1
PV	8	100	2
PV	11	100	2
Genset	15	100	3

the reactive power at node 2, which in turn drives to distribute the reactive power at the PCC among the other levers. As a result, the reactive power diagrams at nodes 6, 8, 11 and 15 exhibit a shape which is rather similar to that of the PCC reactive power diagram.

A number of saturation constraints explain the behavior at the extreme areas of some diagrams. At node 2, the reactive power is limited by the type 1 diagram constraints, which enlightens the behavior for under frequency. Conversely, the type 2 diagram at nodes 8 and 11 constrains the reactive power generation. The generator at node 15 cannot be shut down and the active power is nonzero even for frequencies over 1.04 pu. Finally, the microgrid voltage constraints limits the reactive power generation for the solar panels when the PCC voltage is close to 1 pu. and extreme frequencies (note that the PV active power is not curtailed).

TABLE IV
LINE PARAMETERS

Type	**R [Ohm]**	**X [Ohm]**
1	0.170	0.087
2	0.280	0.087
3	0.353	0.091

TABLE V
LINE CHARACTERISTICS

Line		**Type**	**Length [m]**
From	**To**		
1	2	3	45
2	3	3	50
3	4	3	50
4	5	3	75
5	6	3	75
6	7	3	85
7	8	3	45
8	9	2	95
9	10	2	35
3	11	2	30
4	12	3	20
12	13	3	25
13	14	2	125
14	15	2	85
6	16	2	125
10	18	1	45
17	9	2	85

When the operating point is outside of the PCC capability diagram, it is interesting to focus on the impact of λ_p and λ_q on the active and reactive power provision. λ_p and λ_q weigh respectively the priority to frequency or voltage support in the criterion defined in (8). Table I presents the active and reactive power injections at the PCC for different ratio $\frac{\lambda_q}{\lambda_p}$ and a specified operating point $P_{pcc} = 2.189$ pu, $Q_{pcc} = 2.678$ pu which lies outside the diagram. It can be seen that a high ratio (higher than 10) generates a small reactive and a high active power error. The converse holds for a small ratio. A ratio of 1 minimizes the error on the apparent power.

B. Inclusion of Non-Controlled DER

In the first test case, each of the flexibilities were entirely controlled both in active and in reactive power injections. In this second test case, the reactive power support at node 8 is assumed to be controlled by a linear local control law, namely a reactive power droop. The local droop coefficient can be inferred from the reactive power capacity of the PV inverters (± 0.36 pu, see Fig. 4) and results in a linear gain of 7.2.

Fig. 12 presents the resulting behavior of the PCC. On overall, the behavior remains linear, as expected for a droop-like PCC. The changes appear on the reactive power injection of the PV at node 6. Fig. 13 presents the voltage node 8 (left) and the resulting reactive power injection (right), according to the specified local droop gain. It is interesting to point out that the voltage at node 6 resulting from the optimization routine is mostly dependent of the system frequency and of the active power injections within the micro-grid. Last, the corresponding reactive power is modulated based on the local voltage which does not represent the PCC voltage. This effect

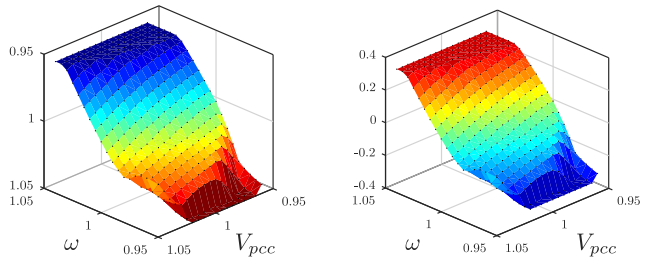

Fig. 13. Voltage node (left) and reactive power injection (right) at node 6 as function of the system frequency and PCC voltage3.

can be explained by the low $\frac{X}{R}$ ratio and the inverse coupling, compared to conventional power system, for which the droop mechanism has been established. This highlights the inability of usual droop relations to enforce accurately the specified behavior at the PCC.

V. Conclusion

A new external droop algorithm has been proposed to achieve the primary control of networked multi-microgrids with multiple DERs. This hierarchical framework only requires the frequency and the PCC voltage signals. The PCC capability diagrams, which vary with the PCC voltage can be found from the grid model and DERs capability diagrams, and the maximum achievable droop gains are computed using power margins. Next, an OPF generates new nonlinear primary control laws of the DERs which achieve the desired behavior at the PCC, while sharing fairly the control effort among the levers. The results obtained with a modified CIGRE benchmark are consistent with intuitive rules.

Further works will focus on the case of a microgrid connected through more than one PCC to one or more external power systems. The estimation of the microgrid capabilities at the PCC can be extended to the case of a microgrid with two or more PCCs. The objective function can be upgraded and embeds weighting factors which will correspond to an allocation of the flexibilities between the different PCCs. Once the PCC PQ diagrams are obtained, the last step in which the local control laws are computed remains the same as in this paper.

The proposed algorithm can consider the uncertainties in both steps of the methodology that is the estimation of the microgrid capabilities at the PCC and the tuning of the local control laws. First, regarding the estimation of the microgrid capabilities at the PCC, the uncertainties can directly be handled by embedding the probability density functions in the optimization routine. This results in an additional dimension of the capability diagram (that is, a three dimensional diagram) which captures the probability of the microgrid to be able to modulate its active and reactive power flows. Second, addressing the uncertainties in the computation of the local control laws requires to change the optimization problem. A linear microgrid network should be considered in order to ensure the global convergence of a confidence level optimization problem as proposed in [31]. The consideration of the uncertainties is a major concern for power system operations and represents the major perspectives of this work.

References

[1] R. Lasseter, "MicroGrids," in *Proc. IEEE Power Eng. Soc. Winter Meeting Conf. (Cat. No.02CH37309)*, vol. 1. New York, NY, USA, 1999, pp. 305–308.

[2] A. Bidram and A. Davoudi, "Hierarchical structure of microgrids control system," *IEEE Trans. Smart Grid*, vol. 3, no. 4, pp. 1963–1976, Dec. 2012.

[3] R. H. Lasseter, "Smart distribution: Coupled microgrids," *Proc. IEEE*, vol. 99, no. 6, pp. 1074–1082, Jun. 2011.

[4] M. N. Alam, S. Chakrabarti, and A. Ghosh, "Networked microgrids: State-of-the-art and future perspectives," *IEEE Trans. Ind. Informat.*, vol. 15, no. 3, pp. 1238–1250, Mar. 2019.

[5] A. G. Tsikalakis and N. D. Hatziargyriou, "Centralized control for optimizing microgrids operation," *IEEE Trans. Energy Convers.*, vol. 23, no. 1, pp. 241–248, Mar. 2008.

[6] D. T. Nguyen and L. B. Le, "Optimal bidding strategy for microgrids considering renewable energy and building thermal dynamics," *IEEE Trans. Smart Grid*, vol. 5, no. 4, pp. 1608–1620, Jul. 2014.

[7] A. D. Hawkes and M. A. Leach, "Modelling high level system design and unit commitment for a microgrid," *Appl. Energy*, vol. 86, nos. 7–8, pp. 1253–1265, 2009.

[8] X. Zhou *et al.*, "A microgrid cluster structure and its autonomous coordination control strategy," in *Proc. IEEE 43rd Annu. Conf. Ind. Electron. Soc. (IECON)*. Beijing, China, Oct. 2017, pp. 2332–2337.

[9] G. De Carne, G. Buticchi, M. Liserre, and C. Vournas, "Real-time primary frequency regulation using load power control by smart transformers," *IEEE Trans. Smart Grid*, vol. 10, no. 5, pp. 5630–5639, Sep. 2019.

[10] M. J. Hossain, M. A. Mahmud, F. Milano, S. Bacha, and A. Hably, "Design of robust distributed control for interconnected microgrids," *IEEE Trans. Smart Grid*, vol. 7, no. 6, pp. 2724–2735, Nov. 2016.

[11] R. Majumder, A. Ghosh, G. Ledwich, and F. Zare, "Power management and power flow control with back-to-back converters in a utility connected microgrid," *IEEE Trans. Power Syst.*, vol. 25, no. 2, pp. 821–834, May 2010.

[12] E. Pashajavid, A. Ghosh, and F. Zare, "A multimode supervisory control scheme for coupling remote droop-regulated microgrids," *IEEE Trans. Smart Grid*, vol. 9, no. 5, pp. 5381–5392, Sep. 2018.

[13] F. Shahnia, A. Ghosh, S. Rajakaruna, and R. P. Chandrasena, "Primary control level of parallel distributed energy resources converters in system of multiple interconnected autonomous microgrids within self-healing networks," *IET Gener. Transm. Distrib.*, vol. 8, no. 2, pp. 203–222, Feb. 2014.

[14] R. Zamora and A. K. Srivastava, "Multi-layer architecture for voltage and frequency control in networked microgrids," *IEEE Trans. Smart Grid*, vol. 9, no. 3, pp. 2076–2085, May 2018.

[15] T. Zhang and H. B. Gooi, "Hierarchical MPC-based energy management and frequency regulation participation of a virtual power plant," in *Proc. IEEE PES Innovat. Smart Grid Technol. Eur.*, Istanbul, Turkey, Oct. 2014, pp. 1–5.

[16] D. Fooladivanda, M. Zholbaryssov, and A. D. Dominguez-Garcia, "Control of networked distributed energy resources in grid-connected AC microgrids," *IEEE Trans. Control Netw. Syst.*, vol. 5, no. 4, pp. 1875–1886, Dec. 2018.

[17] D. Pudjianto, C. Ramsay, and G. Strbac, "Virtual power plant and system integration of distributed energy resources," *IET Renew. Power Gener.*, vol. 1, no. 1, pp. 10–16, Mar. 2007.

[18] X. Wu, J. He, Y. Xu, J. Lu, N. Lu, and X. Wang, "Hierarchical control of residential HVAC units for primary frequency regulation," *IEEE Trans. Smart Grid*, vol. 9, no. 4, pp. 3844–3856, Jul. 2018.

[19] *Technical Requirements for the Connection to and Parallel Operation With Low-Voltage Distribution Networks*, Standard VDE-AR-N 4105, 2019.

[20] J. P. Silva *et al.*, "Estimating the active and reactive power flexibility area at the TSO-DSO interface," *IEEE Trans. Power Syst.*, vol. 33, no. 5, pp. 4741–4750, Sep. 2018.

[21] D. A. Contreras and K. Rudion, "Improved assessment of the flexibility range of distribution grids using linear optimization," in *Proc. 20th Power Syst. Comput. Conf. (PSCC 2018)*, Dublin, Ireland, 2018, pp. 1–7.

[22] T. Lund, P. Sørensen, and J. Eek, "Reactive power capability of a wind turbine with doubly fed induction generator," *Wind Energy*, vol. 10, no. 4, pp. 379–394, 2007.

[23] *Modalités Du Contrôle De Performances Des Installations De Production Raccordées En haute Tension (HTA) Au réseau Public De Distribution Géré par ERDF*, Enedis, Place des Corolles, 2012.
[24] L.-Y. Lu and C.-C. Chu, "Consensus-based droop control synthesis for multiple DICs in isolated micro-grids," *IEEE Trans. Power Syst.*, vol. 30, no. 5, pp. 2243–2256, Sep. 2015.
[25] A. Engler and N. Soultanis, "Droop control in LV-grids," in *Proc. Int. Conf. Future Power Syst.*, Amsterdam, The Netherlands, 2005, p. 6.
[26] X. Hou, Y. Sun, W. Yuan, H. Han, C. Zhong, and J. Guerrero, "Conventional $p - \omega/q - v$ droop control in highly resistive line of low-voltage converter-based AC microgrid," *Energies*, vol. 9, no. 11, p. 943, Nov. 2016.
[27] *Network Code on Requirements for Grid Connection of Generators*, Eur. Comm., Brussels, Belgium, Jul. 2009.
[28] J. W. Simpson-Porco, F. Dorfler, F. Bullo, Q. Shafiee, and J. M. Guerrero, "Stability, power sharing, & distributed secondary control in droop-controlled microgrids," in *Proc. IEEE Int. Conf. Smart Grid Commun. (SmartGridComm)*, Vancouver, BC, Canada, Oct. 2013, pp. 672–677.
[29] J. Schiffer, R. Ortega, A. Astolfi, J. Raisch, and T. Sezi, "Conditions for stability of droop-controlled inverter-based microgrids," *Automatica*, vol. 50, no. 10, pp. 2457–2469, 2014.
[30] K. Strunz *et al.*, "Benchmark systems for network integration of renewable energy resources," CIGRE, Paris, France, Rep. 575, 2014.
[31] J. Buire, F. Colas, J.-Y. Dieulot, L. D. Alvaro, and X. Guillaud, "Confidence level optimization of DG piecewise affine controllers in distribution grids," *IEEE Trans. Smart Grid*, vol. 10, no. 6, pp. 6126–6136, Nov. 2019.

Martin Legry (Member, IEEE) was born in Lille, France, in 1990. He received the Ph.D. degree in electrical engineering from the University of Lille in 2019. His main research interests include the control and the optimization of micro-grids.

Jean-Yves Dieulot was born in Paris, France, in 1968. He received the M.Sc. degree from the Institut Industriel du Nord, France, in 1990, and the Ph.D. and Habilitation Diriger des Recherches degrees in automatic control from the University of Lille, France, in 1993 and 2007, respectively. He is an Associate Professor with Polytech-Lille and CRIStAL, Laboratory of Automatic Control and Computer Sciences of Lille. His research interests are the design of energy-based and nonlinear controllers, and mainly applied to power systems.

Frédéric Colas (Member, IEEE) was born in Lille, France, in October 1980. He received the Ph.D. degree in control system from the École Centrale de Lille, France, in 2007. He is a Member of the Laboratory of Electrotechnics and Power Electronics, Lille, and a Research Engineer with Arts et Métiers Paristech, Lille. His field of interests include the integration of dispersed generation systems in electrical grids, advanced control techniques for power system, and hardware-in-the-loop simulation.

Christophe Saudemont received the Ph.D. degree in electrical engineering from the University of Lille in 1999. From 2001 to 2013, he was a Lecturer and Researcher with Ecole des Hautes Etudes d'Ingénieur, Lille, attached to the Laboratory of Electrotechnics and Power Electronics, Lille. His research activity focuses on intelligent electrical networks (from distribution power system to buildings). He develops energy management strategies, from the DSO and users points of view, integrating sociological, and economic issues of the different actors connected to this network. He participates in the development of full-scale smart-grids demonstrators in the heart of the Catholic University of Lille. He is responsible for the Electrical Networks—Intelligent Transport Research Division of HEI.

Olivier Ducarme received the Electrical Engineer degree from Mons University, Belgium, and the M.B.A. degree from Solvay Business School, Brussels, Belgium. He has been working for different entities of Engie Group: Head of the Low Voltage Department, Tractebel Engineering from July 1995 to July 2001, a Analyst for energy trading business with Risk Assets and Liabilities Management, Electrabel from August 2001 to October 2005, a Forecasting Manager with Electrabel from November 2005 to August 2009, the Head of the Portfolio Economic Studies for Energy Management BU, Engie Corporate from September 2009 to January 2012, and has been the Technology Manager and a Senior Project Manager with Power Networks, Laborelec since February 2012. His main research interests are related to micro-grids.